Chalcogenide Letters

Tech Science Press

http://doi.org/10.32604/cl.2026.077885

ARTICLE

# Enhancement of Thermoelectric Properties in N-Type and P-Type Ag–Te Nanocomposites via Stirring-Assisted Hydrothermal Synthesis

**Donghyeon Lee[#], Jiu Kim[#], Yong-Wook Jeong[#], Miso Shin and Yong Jin Jeong[*]**

Department of Materials Science and Engineering, Korea National University of Transportation, Chungju, Republic of Korea
*Corresponding Author: Yong Jin Jeong. Email: yjjeong@ut.ac.kr
[#]These authors contributed equally to this work

Received: 18 December 2025; Accepted: 03 February 2026; Published: 28 February 2026

**ABSTRACT:** Silver tellurides (Ag–Te) are promising low-temperature thermoelectric materials because their transport properties can be tuned by subtle compositional variations and nanostructuring. Here, we report a stirring-assisted hydrothermal route that enables controlled synthesis of n-type and p-type Ag–Te nanostructures by adjusting the Ag:Te precursor ratio and hydrodynamic conditions. Samples with Ag:Te ratios of 2:1 (Ag2/Te1) and 1:2 (Ag1/Te2) were synthesized at 120°C for 12 h, varying the stirring speed from 0 to 2000 rpm. X-ray diffraction confirms $Ag_2Te$ as the dominant phase for Ag2/Te1 across all conditions, while Te-rich Ag1/Te2 forms a composite mainly consisting of Te and Ag-deficient $Ag_{5-x}Te_3$. For morphology control, the stirring speed significantly alters the microstructural network of the Ag–Te. Moderate stirring (~500 rpm) promotes an interconnected nanowire/nanorod network, whereas higher stirring speeds introduce morphological disruption and secondary phases. Finally, room-temperature transport measurements show that 500 rpm maximizes the power factor for both conduction types: 207.31 μW/mK$^2$ for n-type $Ag_2Te$ and 95.83 μW/mK$^2$ for p-type Te/$Ag_{5-x}Te_3$. This work suggests that controlling the molar ratio of precusors and hydrodynamics during synthesis is a critical factor in optimizing the thermoelectric efficiency of silver tellurides.

**KEYWORDS:** Silver telluride; hydrothermal synthesis; thermoelectric; chalcogenide; stirring

## 1 Introduction

Thermoelectric materials capable of directly converting waste heat into electrical energy are key components for sustainable energy harvesting [1,2]. The performance of these materials is evaluated by the dimensionless figure of merit, $ZT = \alpha^2\sigma T/k$, where an high power factor ($PF = \alpha^2\sigma$) is essential for high efficiency [3,4]. Consequently, substantial research has focused on optimizing the trade-off between the Seebeck coefficient ($\alpha$) and electrical conductivity ($\sigma$) through nanostructuring and composition control [5]. Among chalcogenides, silver telluride (Ag–Te) is a promising candidate for near-room-temperature applications due to its narrow bandgap, high electron mobility, and low lattice thermal conductivity [6–9]. A significant advantage of silver chalcogenides is their non-stoichiometric nature; slight adjustments in the Ag/Te ratio can induce sign changes in the Hall coefficient and enable switching between n-type and p-type conduction in $Ag_{2\pm x}Te$ [10,11]. This tunability is crucial for fabricating practical thermoelectric modules, which require both conduction types [1].

To date, various synthesis strategies have been explored to obtain high-performance silver tellurides, including chemical vapor deposition (CVD), co-precipitation, and solvothermal methods [12–14]. While these techniques offer specific advantages in controlling crystallinity or stoichiometry, hydrothermal synthesis

remains highly attractive due to its procedural simplicity, cost-effectiveness, and potential for large-scale production [15,16]. However, conventional static hydrothermal methods often result in uncontrolled agglomeration and inhomogeneous crystal growth. Controlling the hydrodynamics during synthesis offers a potential solution to these issues [17,18]. Introducing mechanical stirring can modulate the diffusion of ions and reaction kinetics, thereby influencing the nucleation and final morphology of the nanostructures [19,20]. However, despite numerous hydrothermal reports on Ag–Te, systematic studies that isolate hydrodynamic stirring effects on Ag–Te phase evolution and thermoelectric transport remain scarce [15,16].

In this study, a facile and scalable stirring-assisted hydrothermal strategy is proposed to optimize the thermoelectric performance of silver telluride nanostructures. Unlike conventional static methods that often result in random agglomeration, this approach utilizes controlled hydrodynamic forces to modulate nucleation kinetics and crystal growth direction. By systematically varying the stirring speed from 0 to 2000 rpm, the correlation between fluid dynamics, microstructural evolution, and charge transport properties was investigated. Furthermore, through precise adjustment of the precursor stoichiometric ratio, both n-type $Ag_2Te$ nanowires and p-type $Te/Ag_{5-x}Te_3$ composites were successfully synthesized within a unified platform, consistent with known Ag–Te phase relations [21,22]. The experimental results demonstrate that an optimal shear field (500 rpm) is critical for establishing a continuous nanowire network, which significantly enhances the power factor by balancing electrical conductivity and the Seebeck coefficient. This work identifies critical hydrodynamic conditions that maximize the power factor for both conduction types, providing new insights into the design of high-performance chalcogenide thermoelectric materials.

## 2 Experimental Details

### *2.1 Synthesis of Ag–Te Thermoelectric Materials*

Silver nitrate ($AgNO_3$) and Sodium tellurite ($Na_2TeO_3$) were used as the Ag and Te precursors, respectively. The conduction type was controlled by adjusting the molar ratio of Ag to Te. A precursor ratio of Ag:Te = 2:1 was used with 4 mmol of $AgNO_3$ and 2 mmol of $Na_2TeO_3$ for n-type (namely, Ag2/Te1 sample), whereas a precursor ratio of Ag:Te = 1:2 was used with 2 mmol of $AgNO_3$ and 4 mmol of $Na_2TeO_3$ for p-type (namely, Ag1/Te2 sample). The precursors were dissolved in 60 mL of deionized water (DIW). Hydrazine hydrate 1.97 mL and ammonium hydroxide solution (1.6 mL) were added as reducing and complexing agents, respectively. The solution was stirred in a Teflon container for 5 min, followed by hydrothermal synthesis at 120°C for 12 h. The synthesis was performed under different stirring conditions: static (drying oven) and dynamic stirring in an oil bath at speeds of 500, 1000, 1500, and 2000 rpm. The schematic illustration showing preparation procedure was shown in Fig. 1.

### *2.2 Post-Processing and Characterization*

The synthesized powders were vacuum filtered using a PVDF filter and washed twice with DIW and Ethanol. The powders were dried in a vacuum oven at 60°C for 12 h. For thermoelectric measurements, the dried powders were agitated in a vial to ensure homogeneity and then pressed into pellets using a hand press at 10 MPa for 10 min. The morphology of the samples was characterized using scanning electron microscopy (SEM, Thermo Scientific Co. prisma E). The X-ray diffraction (XRD, Bruker Co. D8 advance) pattern of sample was measured using Cu-Kα radiation (λ = 1.5406 Å). The Seebeck coefficient (α) and electrical conductivity (σ) were measured at room temperature (RT) using a KEITHLEY 2636B/2182A/2700 system and the four-probe method, respectively, to calculate the power factor ($PF = \alpha^2\sigma$).

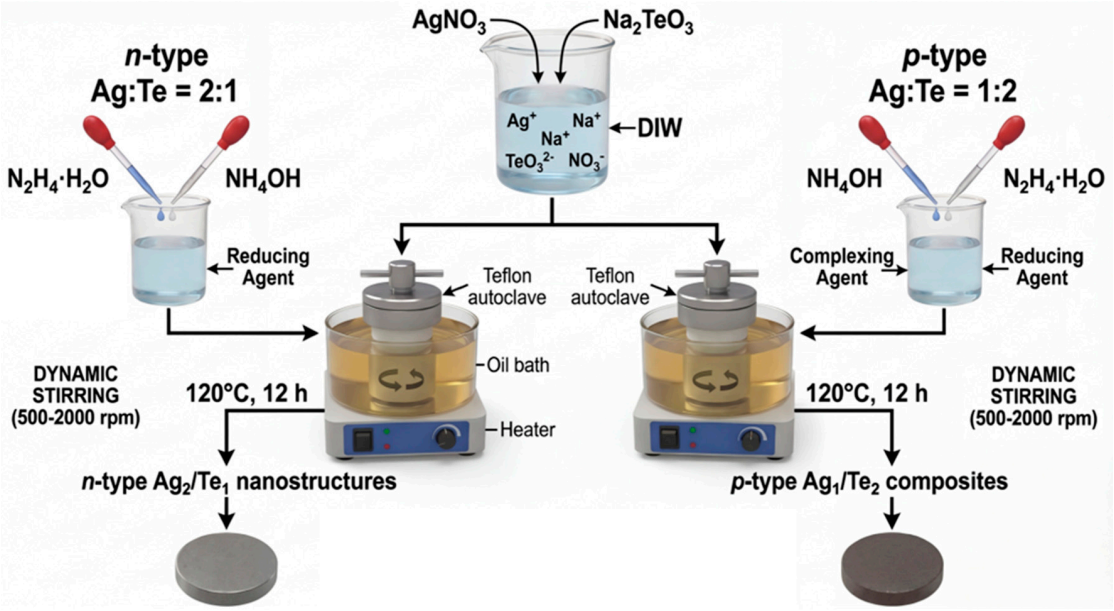


**Figure 1:** Schematic illustration of the stirring-assisted hydrothermal synthesis of Ag–Te nanostructures, followed by pellet preparation for thermoelectric measurements.

## 3 Results and Discussion

The influence of hydrodynamic conditions on the microstructural evolution of silver telluride was systematically investigated using XRD and SEM. Regardless of the Ag2/Te1 samples synthesized in the oven and in the oil bath, the overall XRD pattern (Fig. 2) and crystal parameters (Table 1) remained almost identical and the strong intensity peaks of Ag2/Te1 samples were observed at $2\theta = 31^{\circ}$ and $39^{\circ}$. From comparison with JCPDS #081-1820 $Ag_2Te$, it can be confirmed that $Ag_2Te$ was successfully synthesized under all conditions. Excessive shear forces at speeds above 1000 rpm likely disrupt the chemical equilibrium, leading to the precipitation of secondary Ag phases (JCPDS #004-0783 Ag). In other words, The presence of these trace amounts at high speeds is a result of the extreme hydrodynamic conditions rather than a failure of the synthesis protocol itself. The morphology of the synthesized Ag2/Te1 samples showed a strong dependence on the stirring speed applied during the hydrothermal reaction. As shown in the SEM images for the Ag2/Te1 samples (Fig. 3), the sample synthesized under static conditions (drying oven) exhibited a disordered morphology characterized by random agglomeration of particles. This lack of a defined structure suggests that in the absence of external kinetic energy, crystal growth is limited by the slow diffusion of precursors, resulting in poor connectivity. However, the introduction of mechanical stirring over 500 rpm induced a dramatic transformation. The morphology evolved into a dense network of thin nanowires and nanorods. This interconnected network is critical for thermoelectric applications as it facilitates efficient charge carrier transport while potentially scattering phonons at the grain boundaries. Increasing the stirring speed of 1000, 1500, and 2000 rpm, the SEM micrographs revealed that the growth of the nanowires was confirmed to result in increased length and diameter. However, the excessive shear forces induced by the turbulent flow likely resulted in phase segregation and mechanical breakage, creating regions that hindered efficient charge transport. Structural analysis from the XRD spectra (Fig. 2) indicated that the high-speed conditions (1000 and 2000 rpm) included small signal of Ag (111) peaks, suggesting the formation of secondary phases. Vigorous stirring might alter the chemical equilibrium, leading to phase segregation.

**Table 1:** Crystal parameters of Ag2/Te1 samples synthesized under static (oven) and stirring-assisted hydrothermal conditions (500–2000 rpm).

| Ag2/Te1 Samples | Oven | 500 rpm | 1000 rpm | 1500 rpm | 2000 rpm |
|---|---|---|---|---|---|
| $d_{112}$-spacing (nm) | 2.31 | 2.3 | 2.3 | 2.3 | 2.3 |
| Crystallite size D (nm) | 51.4 | 61.6 | 59.1 | 60.4 | 59.2 |

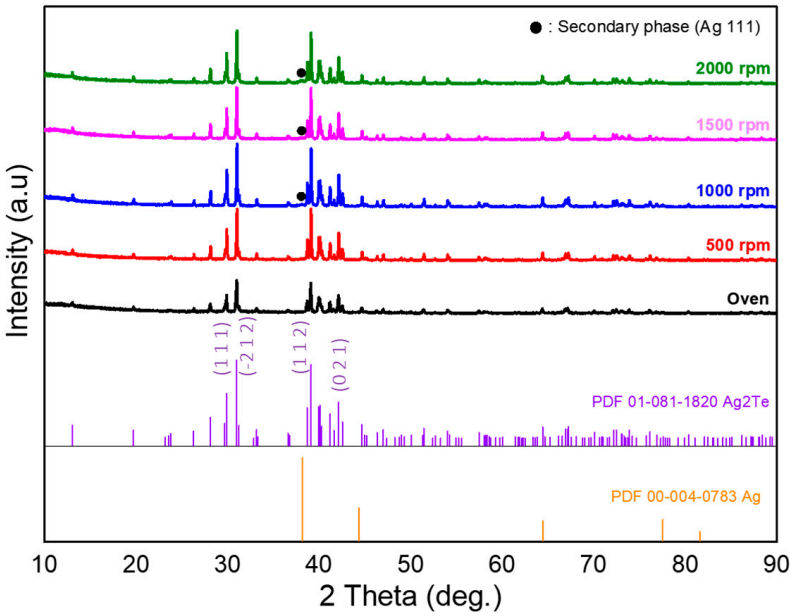


**Figure 2:** XRD patterns (Cu Kα, λ = 1.5406 Å) of Ag2/Te1 samples synthesized under static (oven) and stirring-assisted hydrothermal conditions (500–2000 rpm).

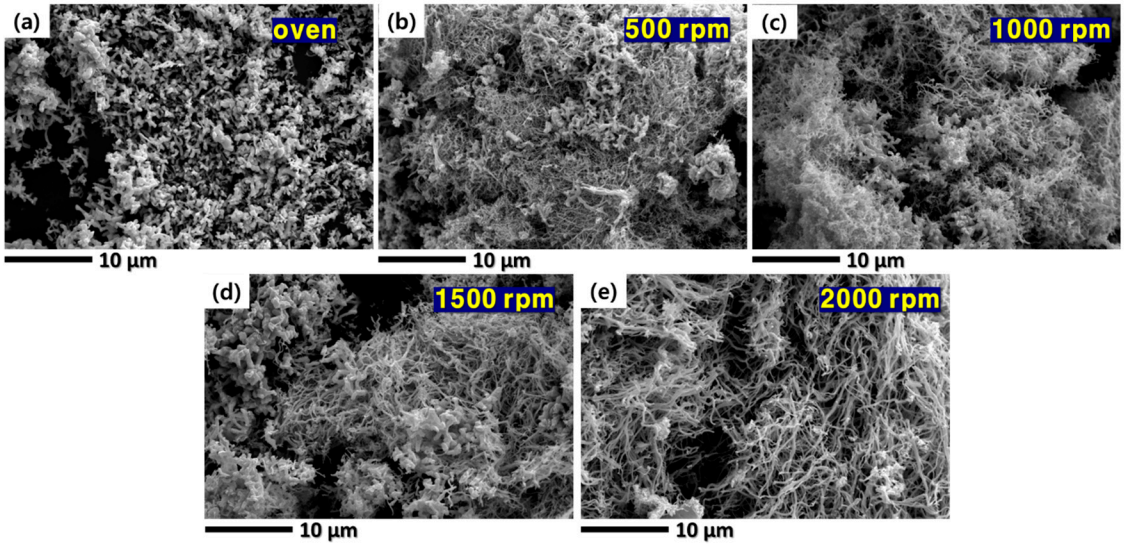


**Figure 3:** SEM micrographs of Ag2/Te1 samples synthesized at different stirring speeds: (**a**) static (oven), (**b**) 500 rpm, (**c**) 1000 rpm, (**d**) 1500 rpm, and (**e**) 2000 rpm.

The Ag1/Te2 samples synthesized with a precursor ratio adjusted to 1:2 was analyzed by XRD under identical conditions. In Fig. 4, the XRD analysis for Ag1/Te2 samples confirmed that the majority of peaks corresponded to the Te phase (with a strong Te peak at 2θ = 27.5°, JCPDS #065-3370) and $Ag_{4.96}Te_3$ (distinct peaks at 2θ = 34.02° and 41.4°, JCPDS #085-9807), with the 500 rpm condition providing the most favorable phase purity for transport. The calculated crystal parameters of $Ag_{4.96}Te_3$ were summarized in Table 2. The presence of Te phase is attributed to the increased Te ratio, which limited its reaction with Ag and led to independent Te growth. Consequently, in the case of the Ag1/Te2 recipe, a composite structure consisting of Te nanowires and Ag-deficient silver telluride $Ag_{5-x}Te_3$ appears to have been synthesized. Fig. 5 presents the SEM analysis of Ag1/Te2 samples synthesized with different reaction conditions. Similar to the Ag2/Te1 sample, the specimen synthesized in the oven exhibited discontinuous particle growth, with Te observed to grow independently in the form of nanorod/wires. In contrast, the stirring-assisted hydrothermal reaction revealed elongated morphologies in which the particles form continuous network structures. As the stirring speed increased, both the $Ag_{5-x}Te_3$ particles and the Te nanowires became thinner and longer, indicating enhanced anisotropic growth under stronger shear conditions. This morphological transition from isolated particles to a continuous nanowire network suggests that the applied shear force is critical for establishing effective electrical percolation pathways within the composite matrix.

**Table 2:** Crystal parameters of Ag1/Te2 samples synthesized under static (oven) and stirring-assisted hydrothermal conditions (500–2000 rpm).

| Ag1/Te2 Samples | Oven | 500 rpm | 1000 rpm | 1500 rpm | 2000 rpm |
|---|---|---|---|---|---|
| $d_{224}$-spacing (nm) | 2.63 | 2.63 | 2.63 | 2.63 | 2.63 |
| Crystallite size D (nm) | 43.72 | 47.79 | 45.46 | 46.44 | 46.47 |

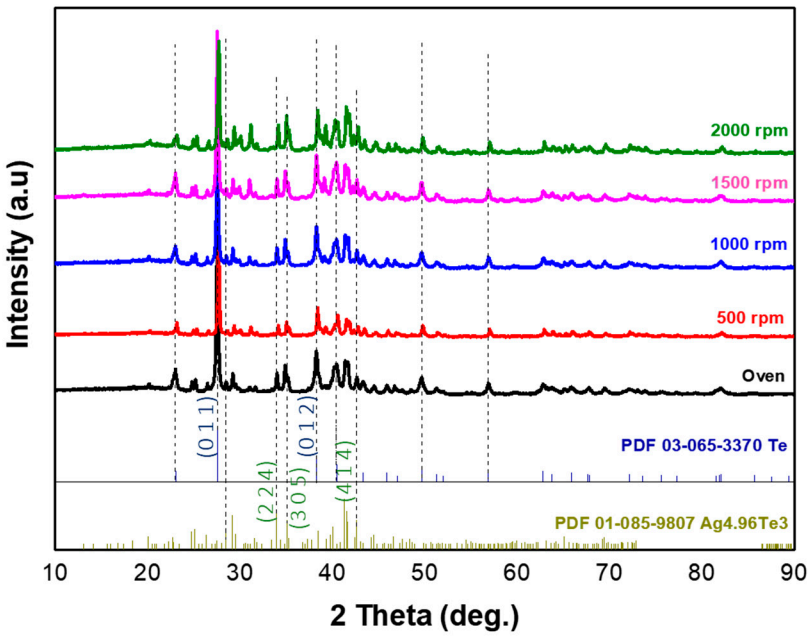


**Figure 4:** XRD patterns (Cu Kα, λ = 1.5406 Å) of Ag1/Te2 samples synthesized under static (oven) and stirring-assisted hydrothermal conditions (500–2000 rpm).

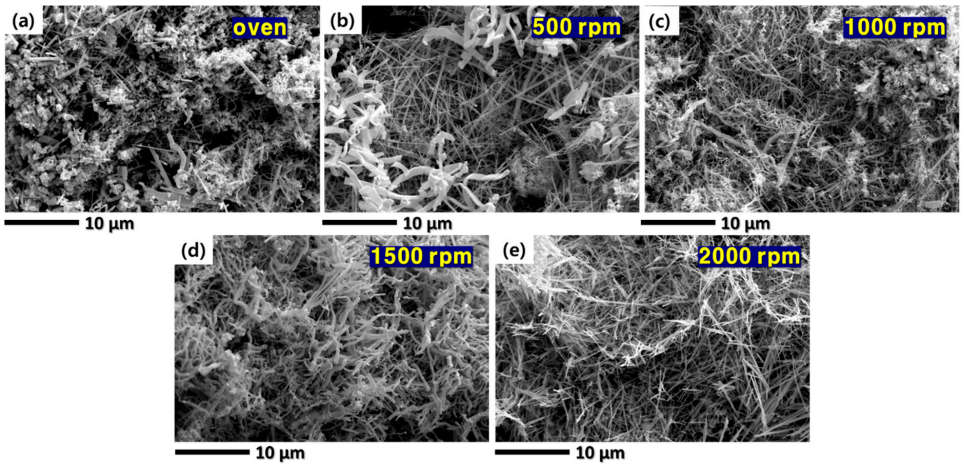


**Figure 5:** SEM micrographs of Ag1/Te2 samples synthesized at different stirring speeds: (**a**) static (oven), (**b**) 500 rpm, (**c**) 1000 rpm, (**d**) 1500 rpm, and (**e**) 2000 rpm.

The structural variations induced by stirring speed directly influenced the thermoelectric transport properties, as quantified in Fig. 6a,b and Table 3. For the $Ag_2Te$ nanowires from the Ag2/Te1, the static synthesis method yielded an n-type semiconductor behavior, with $\alpha$ of −48.52 µV/K and $\sigma$ of 25.56 S/cm. The introduction of stirring at 500 rpm resulted in a remarkable enhancement in both parameters. The $\sigma$ increased to its peak value of 35.99 S/cm, which can be attributed to the formation of the well-connected nanowire network observed in the SEM analysis, providing effective percolation pathways for electrons. Simultaneously, the $\alpha$ improved drastically to −240.01 µV/K, a nearly five-fold increase compared to the static sample. This simultaneous increase suggests that the 500 rpm condition optimized the carrier concentration and mobility without introducing excessive scattering. Further increasing the stirring speed negatively impacted the performance. At 1000 rpm, the $\alpha$ dropped to −136.13 µV/K, and the $\sigma$ decreased to 23.84 S/cm. This downward trend continued at 2000 rpm, where the $\alpha$ plummeted to −46.38 µV/K. This degradation might arise because the appearance of Ag secondary phases and the disruption of the nanowire network at high speed likely introduced defect centers that scatter charge carriers, thereby reducing mobility and the Seebeck effect. Consequently, the *PF*, which represents the overall thermoelectric efficiency, reached a maximum of 207.31 µW/mK$^2$ at 500 rpm. This is significantly higher than the *PF* of the oven sample (6.02 µW/mK$^2$) and the 2000 rpm sample (5.21 µW/mK$^2$), confirming that Ag2/Te1 recipe and 500 rpm is the critical hydrodynamic condition for n-type optimization.

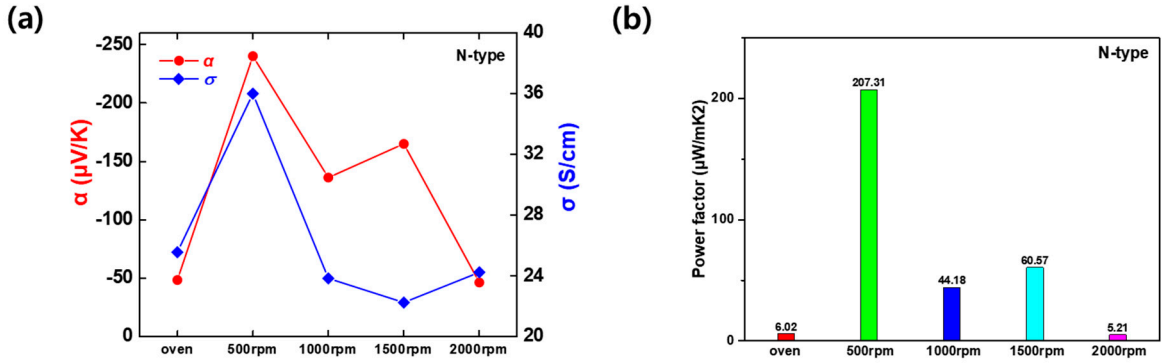


**Figure 6:** *Cont.*

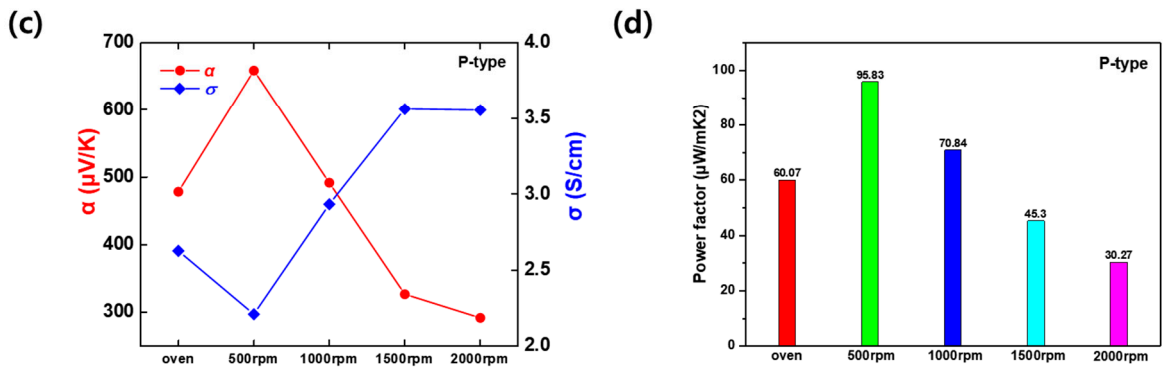


**Figure 6:** Room-temperature thermoelectric properties as a function of stirring speed for (**a**,**b**) Ag2/Te1 (n-type) and (**c**,**d**) Ag1/Te2 (p-type) samples: (**a**,**c**) Seebeck coefficient (α) and electrical conductivity (σ); (**b**,**d**) corresponding power factor (PF = $\alpha^2\sigma$).

**Table 3:** Summary in thermoelectric properties as a function of stirring speed for Ag2/Te1 (n-type) samples.

| Ag2/Te1 (n-Type) Samples | Oven | 500 rpm | 1000 rpm | 1500 rpm | 2000 rpm |
|---|---|---|---|---|---|
| $\alpha$ (μV/K) | −48.52 | −240.01 | −136.13 | −164.98 | −46.38 |
| $\sigma$ (S/cm) | 25.56 | 35.99 | 23.84 | 22.25 | 24.24 |
| *PF* (μW/mK$^2$) | 6.02 | 207.31 | 44.18 | 60.57 | 5.21 |

The Te/$Ag_{5-x}Te_3$ from Ag1/Te2 samples exhibited a similar dependence on stirring speed, confirming the universality of the synthesis protocol. As shown in Fig. 6c,d and Table 4, the positive α corresponded to p-type semiconductor behavior, possibly resulting from the intrinsic properties of the Te-rich phase. The sample synthesized at 500 rpm achieved the highest α of 658.48 μV/K. This is a substantial improvement over the oven-synthesized sample (478.12 μV/K). Unlike the n-type samples ($Ag_2Te$), the σ of the p-type Te/$Ag_{5-x}Te_3$ samples showed a slight upward trend with increasing stirring speed, rising from 2.21 S/cm at 500 rpm to 3.56 S/cm at 1500 rpm. However, the overall conductivity values remained lower than those of the n-type counterparts, generally falling in the range of 2~3 S/cm. Despite the slight increase in conductivity at higher speeds, the drastic reduction in the α severely compromised the overall performance. As the stirring speed increased from 500 rpm to 1000 and 2000 rpm, the α decreased to 491.51 μV/K and 291.90 μV/K, respectively. This trade-off suggests that while high-speed stirring might densify the material slightly to improve conductivity, it simultaneously introduces defects or alters the carrier concentration away from the optimum, leading to a loss in α and thermopower. As a result, the *PF* for Te/$Ag_{5-x}Te_3$ followed the same trend as the n-type, peaking at 500 rpm with a value of 95.83 μW/mK$^2$. The *PF* significantly declined at higher speed, dropping to 30.27 μW/mK$^2$ at 2000 rpm. The phase agreement in the XRD patterns and the abrupt variations in the Seebeck coefficient (including n/p-type transition and behavior) provide sufficient evidence for the crystal structure and chemical state. Collectively, these results demonstrate that the hydrothermal strategy allows for phase tunability—yielding either n-type single-phase $Ag_2Te$ or p-type Te/$Ag_{5-x}Te_3$ composites simply by adjusting the precursor ratio—while a stirring speed of 500 rpm serves as a universal optimum to maximize the thermoelectric performance of both systems.

**Table 4:** Summary in thermoelectric properties as a function of stirring speed for Ag1/Te2 (p-type) samples.

| Ag1/Te2 (p-Type) Samples | Oven | 500 rpm | 1000 rpm | 1500 rpm | 2000 rpm |
|---|---|---|---|---|---|
| $\alpha$ (μV/K) | 478.12 | 658.48 | 491.51 | 326.74 | 291.90 |
| $\sigma$ (S/cm) | 2.63 | 2.21 | 2.93 | 3.56 | 3.55 |
| *PF* (μW/mK$^2$) | 60.07 | 95.83 | 70.84 | 45.30 | 30.27 |

## 4 Conclusion

In this study, it was demonstrated that hydrodynamic control during hydrothermal synthesis is an effective and scalable strategy to optimize the thermoelectric performance of Ag–Te nanostructures. By tuning the Ag:Te precursor ratio, we obtained Ag2/Te1 (Ag:Te = 2:1) with $Ag_2Te$ as the dominant phase and Ag1/Te2 (Ag:Te = 1:2) forming a Te-rich composite mainly consisting of Te and Ag-deficient $Ag_{5-x}Te_3$. SEM indicates that moderate stirring promotes an interconnected nanowire/nanorod network, whereas excessive stirring tends to disrupt connectivity and can introduce secondary features. Thermoelectric measurements reveal a clear optimum at 500 rpm, delivering the highest power factors of 207.31 μW/mK$^2$ (n-type, $Ag_2Te$ nanowires) and 95.83 μW/mK$^2$ (p-type, Te/$Ag_{5-x}Te_3$ composites). These results highlight stirring speed as a critical synthesis parameter that governs the morphology–transport relationship in Ag–Te materials, and they provide practical guidelines for engineering complementary n-type and p-type elements using a unified hydrothermal platform.

**Acknowledgement:** None.

**Funding Statement:** This work was supported by the National Research Foundation of Korea (NRF) grant funded by the Korea government (MSIT) (RS-2024-00405290). This research was also supported by the Regional Innovation System & Education (RISE) program through the (Chungbuk Regional Innovation System & Education Center), funded by the Ministry of Education (MOE) and the (Chungcheongbuk-do), Republic of Korea (2025-RISE-11-004-01).

**Author Contributions:** The authors confirm contribution to the paper as follows: study conception and design: Donghyeon Lee, Jiu Kim; data collection: Yong-Wook Jeong, Miso Shin; analysis and draft manuscript preparation: Yong Jin Jeong. All authors reviewed and approved the final version of the manuscript.

**Availability of Data and Materials:** Not applicable.

**Ethics Approval:** Not applicable.

**Conflicts of Interest:** The authors declare no conflicts of interest.

## References

1. Snyder GJ, Toberer ES. Complex thermoelectric materials. Nat Mater. 2008;7(2):105–14. [CrossRef].
2. Bell LE. Cooling, heating, generating power, and recovering waste heat with thermoelectric systems. Science. 2008;321(5895):1457–61. [CrossRef].
3. Zavanelli D, Pröschel A, Winograd J, Cherkez R, Snyder GJ. When power factor supersedes $zT$ to determine power in a thermocouple. J Appl Phys. 2022;131(11):115101. [CrossRef].
4. Wolf M, Hinterding R, Feldhoff A. High power factor *vs.* high zT—A review of thermoelectric materials for high-temperature application. Entropy. 2019;21(11):1058. [CrossRef].
5. Chen G, Dresselhaus MS, Dresselhaus G, Fleurial JP, Caillat T. Recent developments in thermoelectric materials. Int Mater Rev. 2003;48(1):45–66. [CrossRef].
6. Samal AK, Pradeep T. Room-temperature chemical synthesis of silver telluride nanowires. J Phys Chem C. 2009;113(31):13539–44. [CrossRef].

7. Milenov TI, Tenev T, Miloushev I, Avdeev GV, Luo CW, Chou WC. Preliminary studies of the Raman spectra of $Ag_2Te$ and $Ag_5Te_3$. Opt Quantum Electron. 2013;46:573–80. [CrossRef].
8. Deng Y, Wei M, Lei Y, Lu J, Peng P, Zhang Y, et al. Advances in silver-based chalcogenide flexible thermoelectric materials. Cryst Eng Comm. 2025;27(8):1055–77. [CrossRef].
9. Gautam AK, Khare N. Enhanced thermoelectric figure of merit at near room temperature in n-type binary silver telluride nanoparticles. J Materiomics. 2023;9(2):310–7. [CrossRef].
10. Lee M, Rosenbaum TF, Saboungi ML, Schnyders HS. Band-gap tuning and linear magnetoresistance in the silver chalcogenides. Phys Rev Lett. 2002;88(6):066602. [CrossRef].
11. Wuliji H, Zhao K, Cai X, Jing H, Wang Y, Huang H, et al. Study of the defect chemistry in Ag2Q (Q = S, Se, Te) by first-principles calculations. Mater Today Phys. 2023;35:101129. [CrossRef].
12. Lee HH, Lee S, Hwang G, Lee S, Cho S. Vapor–liquid–solid synthesis of $Ag_2Te$ using chemical vapor deposition method. APL Mater. 2024;12:011123. [CrossRef].
13. Kadim AM, Abass KH. Synthesis of silver telluride nanoparticles via chemical co-precipitation method for antibacterial applications. Iraqi J Appl Phys. 2025;21(3):317–22. [CrossRef].
14. OuYang WJ, Liang CM, Koo MC, Zhao PY, Wang GS. Facile synthesis of novel one-dimensional silver telluride heterojunction composite with superior electromagnetic wave attenuation capacity. Nano Res. 2025;18(12):94907976. [CrossRef].
15. Chang Y, Guo J, Tang YQ, Zhang YX, Feng J, Ge ZH. Facile synthesis of $Ag_2Te$ nanowires and thermoelectric properties of $Ag_2Te$ polycrystals sintered by spark plasma sintering. Cryst Eng Comm. 2019;21(11):1718–27. [CrossRef].
16. Manzoor S, Liu Y, Yu Z, Fu X, Ban G. Hydrothermal synthesis and mechanism of unusual zigzag $Ag_2Te$ and $Ag_2Te$/C core-shell nanostructures. J Nanomater. 2014;2014:350981. [CrossRef].
17. Szterner P, Biernat M. Effect of reaction time, heating and stirring rate on the morphology of HAp obtained by hydrothermal synthesis. J Therm Anal Calorim. 2022;147(23):13059–71. [CrossRef].
18. Hamao N, Itasaka H, Mimura K, Liu Z, Hamamoto K. Effect of stirring on particle shape and size in hydrothermal synthesis of $LiCoO_2$. ACS Omega. 2024;9;23597–602. [CrossRef].
19. Chandima Pradeep EK, Chauvel A, Abdurrahmanoglu C, Kiebach R, Bjørnetun Haugen A. Effect of stirring and KOH/NaOH ratio on phase formation in hydrothermal synthesis of $KNbO_3$-$NaNbO_3$ particles. J Supercrit Fluids. 2024;212:106340. [CrossRef].
20. Dong R, Wang F, Jing D, Liu Y, Bao Y. The stirring effect on the crystal morphology of p-acetamidobenzoic acid solution crystallization. Crystals. 2025;15(3):284. [CrossRef].
21. Karakaya I, Thompson WT. The Ag-Te (silver-tellurium) system. J Phase Equilib. 1991;12(1):56–63. [CrossRef].
22. Voronin MV, Osadchii EG, Brichkina EA. Thermochemical properties of silver tellurides including empressite (AgTe) and phase diagrams for Ag–Te and Ag–Te–O. Phys Chem Miner. 2017;44(9):639–53. [CrossRef].